Journal of Computational Physics 228 (2009) 1172–1187

Contents lists available at ScienceDirect

Journal of Computational Physics

journal homepage: www.elsevier.com/locate/jcp

Efficient computation of the spectrum of viscoelastic flows

J.V. Valério [a], M.S. Carvalho [b,*], C. Tomei [a]

[a] Departamento de Matemática, Pontificia Universidade Catolica do Rio de Janeiro, Rua Marques de Sao Vicente 225, Gavea 22453-900, Rio de Janeiro, RJ, Brazil
[b] Departamento de Engenharia Mecânica, Pontificia Universidade Catolica do Rio de Janeiro, Rua Marques de Sao Vicente 225, Gavea 22453-900, Rio de Janeiro, RJ, Brazil

ARTICLE INFO

Article history:
Received 14 May 2008
Received in revised form 18 September 2008
Accepted 12 October 2008
Available online 1 November 2008

Keywords:
Incompressible flows
Stability analysis
Eigenvalues at infinity
Finite elements

ABSTRACT

The understanding of viscoelastic flows in many situations requires not only the steady state solution of the governing equations, but also its sensitivity to small perturbations. Linear stability analysis leads to a generalized eigenvalue problem (GEVP), whose numerical analysis may be challenging, even for Newtonian liquids, because the incompressibility constraint creates singularities that lead to non-physical *eigenvalues at infinity*. For viscoelastic flows, the difficulties increase due to the presence of continuous spectrum, related to the constitutive equations.

The Couette flow of upper convected Maxwell (UCM) liquids has been used as a case study of the stability of viscoelastic flows. The spectrum consists of two discrete eigenvalues and a continuous segment with real part equal to $-1/We$ (*We* is the Weissenberg number). Most of the approximations in the literature were obtained using spectral expansions. The eigenvalues close to the continuous part of the spectrum show very slow convergence.

In this work, the linear stability of Couette flow of a UCM liquid is studied using a finite element method. A new procedure to eliminate the eigenvalues at infinity from the GEVP is proposed. The procedure takes advantage of the structure of the matrices involved and avoids the computational overhead of the usual mapping techniques. The GEVP is transformed into a non-degenerate GEVP of dimension five times smaller. The computed eigenfunctions related to the continuous spectrum are in good agreement with the analytic solutions obtained by Graham [M.D. Graham, Effect of axial flow on viscoelastic Taylor–Couette instability, J. Fluid Mech. 360 (1998) 341].

1. Introduction

Linear stability analysis of incompressible flows is used in many practical examples to determine the parameters at which the flow becomes unstable. It is an important design tool for many manufacturing processes, where a steady state flow is crucial for uniform product quality.

The hydrodynamic stability of a laminar flow is determined by tracking the effect of a perturbation of the flow. The discretization of the system of linear differential equations that describe the amplitude of the perturbations $\mathbf{c}$ and its rate of growth σ leads to a non-Hermitian, generalized eigenvalue problem (GEVP) of the form

$$\mathbf{Jc} = \sigma\mathbf{Mc}. \tag{1}$$

The matrices $\mathbf{J}$ and $\mathbf{M}$ are usually called the *Jacobian* and *mass matrices*.

* Corresponding author. Tel.: +55 21 35271174; fax: +55 21 35271165.
E-mail address: msc@puc-rio.br (M.S. Carvalho).

0021-9991/$ - see front matter © 2008 Elsevier Inc. All rights reserved.
doi:10.1016/j.jcp.2008.10.018

The challenges of linear stability analyses of viscoelastic flows are many. The presence of elastic stress boundary layers requires a refined mesh in some regions of the flow, leading to large matrices. The differential models used to describe the viscoelastic behavior of liquids lead to singularities. In contrast to Newtonian flows, the related linear eigenvalue problem may contain continuous spectrum in addition to discrete eigenvalues.

These difficulties are already present in the stability analysis of simple Couette flow of an upper convected Maxwell (UCM) liquid. In their theoretical analysis of a simple geometry, Gorodtsov and Leonov [1] showed that the related spectrum is composed by the so called Gorodtsov–Leonov eigenvalues, and an interval in the complex plane given by $-1/We \pm i\alpha U$, where We is the Weissenberg number, α is the wavenumber of the perturbation along the flow direction and U is the wall velocity. The literature contains a number of texts dedicated to the numerical confirmation of their description, along with generalizations to different rectilinear flows, such as Poiseuille and multilayered flows, together with more elaborate constitutive models. Important contributions can be found in [2–6,8]. In these analysis, the flow perturbation along the cross-stream direction is written in terms of the streamfunction and spectral methods are then used to solve the equations.

Previous numerical experiments recover very well the Gorodtsov–Leonov eigenvalues and approximate the continuous spectrum by oval-shaped figures. The width of the oval figure decreases for denser discretizations, but convergence is slow, as seen in [3–5]. As commented by several authors, the inaccurate approximation of the continuous spectrum and the slow convergence of these eigenmodes are related to the singular nature of the eigenfunction. There are two known families of eigenfunctions related to the continuous spectrum of this flow. Graham [10] obtained two-dimensional subspaces of solutions that have non-zero velocity field and non-integrable singular stress fields. This is consistent with the presence of ovals in numerical experiments. Kupferman [11] found another family of distribution-valued eigenfunctions for the stress field, consisting of delta functions and their derivatives, which do not perturb the velocity field. He also considered the effect of the finite-difference scheme on the numerical approximation of the continuous spectrum. At high Weissenberg numbers, the real part of the continuous spectrum is a small negative number, whereas their approximations by the oval may cross the imaginary axis, leading to incorrect predictions about the stability of the flow.

Solving the GEVP (1) may be difficult even for viscous flows. The discretization describing the perturbed fields leads to large matrices, frequently ruling out the calculation of the full spectrum. Only the leading eigenvalues, those with the largest real part, are calculated, usually by iterative methods. Moreover, the mass matrix $\mathbf{M}$, associated to the transient terms of the governing equations, is singular because the mass conservation equation of incompressible flows does not have a transient term. This singularity gives rise to (theoretical) eigenvalues at infinity, which manifest in computations as large, but finite, numbers.

Large eigenvalues have to be tamed: naive iterative methods favor the eigenvalues with the largest modulus, not those with the largest real part. To circumvent this difficulty, a common procedure is to use a shift-and-invert transformation, mapping infinity to zero, as done by Sureshkumar and Beris [3]. Iterative methods used to solve the transformed problem will favor the eigenvalues closest to the shift parameter, not the leading ones. Christodoulou and Scriven [12] used approximately exponential preconditioning by rational transformation to overcome these difficulties. In this case, the eigenvalues of the transformed problem are the exponentials of the original eigenvalues, and thus eigenvalues of largest real part in the original problem give rise to eigenvalues of largest modulus in the transformed problem, and standard iteration techniques, like the many variations of Arnoldi's method, may be considered. The preconditioning step is computationally expensive. Navarro et al. [7] developed an efficient method based on a modified Cayley transformation followed by another transformation for the eigenvalues at infinity to solve the generalized eigenvalue problem that describes the linear stability of a fluid heated non-uniformly from bellow. However, as they stated, some care needs to be taken since not all the eigenvalues at infinity are removed.

Taking a different approach, Arora and Sureshkumar [8] accurately captured the spectrum in the purely elastic limit for an Oldroyd-B liquid, with substantial reduction in CPU time and memory requirements. Their algorithm, however, can only be applied to creeping flows (i.e., vanishing Reynolds number) and constitutive models with a polymeric viscosity term. In particular, it cannot be applied to a UCM liquid. To avoid these limitations, Sureshkumar [9] presented his compressible viscoelastic formulation (CVF), which is well suited for the linear stability analysis of viscoelastic flows. The incompressible eigensolutions can be recovered from CVF in the limit of small compressibility. In essence, CVF is a penalty-formulation to remove the singularity of the mass matrix.

Valerio et al. [13] showed that the GEVP resulting from linear stability analysis of viscous flows may be reduced to a smaller non-singular GEVP. The linear stability analysis is formulated in terms of the primitive variables, namely, pressure, stress tensor and velocity of the flow. The differential equations are discretized using finite elements. In this work, an extension of this procedure is proposed for the Couette flow of an UCM liquid. By keeping track of the sources of eigenvalues at infinity combined with a detailed analysis of the structure of the mass and Jacobian matrices, eigenvalues at infinity are eliminated by an algebraic procedure. As a consequence, the original (GEVP) becomes five times smaller and the new mass matrix is non-singular. The numerical computation of the spectrum is very satisfactory, with substantial savings in memory requirements and CPU time. The discretization of the continuous spectrum gives rise to a peculiar picture, which at first sight suggests three different arcs of eigenvalues, the middle one lying on top of the continuous spectrum. Careful examination, however, shows that only two discrete eigenvalues appear for a fixed imaginary part: one on the central arc, the other alternating from left to right. The related eigenfunctions are in good agreement with the analytical solutions presented by Graham. This peculiar pattern seems due to the choice of element discretization: eigenfunctions and eigenvalues are significatively related to the underlying mesh and basis functions.

2. Linear stability analysis: finite elements discretization

The velocity $\mathbf{v}$ and pressure p fields of steady state, incompressible, creeping flow are governed by the continuity and momentum equations

$$\nabla \cdot \mathbf{v} = 0, \quad -\nabla p + \nabla \cdot \boldsymbol{\tau} = 0.$$

The extra-stress tensor is $\boldsymbol{\tau}$. In order to compare the predictions with previous work in the literature, the upper convected Maxwell (UCM) constitutive equation was chosen to represent the viscoelastic behavior of the liquid

$$\boldsymbol{\tau} + We\boldsymbol{\tau}_{(1)} = \dot{\gamma},$$

where $\boldsymbol{\tau}_{(1)} = (\mathbf{v}\cdot\nabla)\boldsymbol{\tau} - (\nabla\mathbf{v})\boldsymbol{\tau} - \boldsymbol{\tau}(\nabla\mathbf{v})^T$ is the upper convected derivative and $\dot{\gamma} = (\nabla\mathbf{v} + \nabla\mathbf{v}^T)$ is the rate-of-strain tensor. The Weissenberg number is $We \equiv V\lambda/L$ and λ is the relaxation time of the liquid. The gradient of the velocity is given by the matrix $\nabla\mathbf{v} = \frac{\partial v_i}{\partial x_j} e_i e_j$.

Geometry and boundary conditions are shown in Fig. 1. Liquid flows between two parallel plates located at $y = \pm 1$ that are moving with velocity $U = \pm 1$. Gorodtsov and Leonov [1] considered a similar geometry. The steady state solution of this problem is given by

$$\mathbf{v_0} = (y, 0, 0), \quad p_0 = 0 \quad \text{and} \quad \tau_0 = \begin{bmatrix} 2We & 1 & 0 \\ 1 & 0 & 0 \\ 0 & 0 & 0 \end{bmatrix}.$$

To determine its linear stability, we add perturbations to the fields above,

$$\mathbf{v}(\mathbf{x}, t) = \mathbf{v_0}(\mathbf{x}) + \epsilon\, \mathbf{v}'(y) e^{i\alpha x + \sigma t},$$

$$p(\mathbf{x}, t) = p_0(\mathbf{x}) + \epsilon\, p'(y) e^{i\alpha x + \sigma t},$$

$$\boldsymbol{\tau}(\mathbf{x}, t) = \boldsymbol{\tau}_0(\mathbf{x}) + \epsilon\, \boldsymbol{\tau}'(y) e^{i\alpha x + \sigma t}.$$

The fields $\mathbf{v}', p'$ and $\boldsymbol{\tau}'$ describe amplitudes and σ is the growth factor of the perturbation. The wave number α along the flow direction is given; in applications, stability is considered for a range of values. As usual, the sign of $\Re(\sigma)$, the real part of σ, determines the stability of the flow. Thus, $\mathbf{v}$, p and $\boldsymbol{\tau}$ satisfy

$$\nabla \cdot \mathbf{v} = 0, \quad -\nabla p + \nabla \cdot \boldsymbol{\tau} = 0, \quad \boldsymbol{\tau} + We\ \boldsymbol{\tau}_{(1)} = \dot{\gamma}, \tag{2}$$

where now $\boldsymbol{\tau}_{(1)} = \frac{\partial \boldsymbol{\tau}}{\partial t} + (\mathbf{v}\cdot\nabla)\boldsymbol{\tau} - (\nabla\mathbf{v})\boldsymbol{\tau} - \boldsymbol{\tau}(\nabla\mathbf{v})^T$ is the upper convected derivative with an additional transient term.

Following the usual procedure, we insert in the system (2) the expressions for the perturbed fields and neglect terms of order $\mathcal{O}(\epsilon^2)$, on our way to compute the sensitivity matrix related to the linear stability of the flow. To simplify notation, we drop primes: the perturbed fields will be represented by $p, \boldsymbol{\tau}$, and $\mathbf{v}$. We list the three different types of equations: for continuity, for the UCM constitutive model and, finally, for momentum conservation:

$$\begin{aligned}
&i\alpha u + \frac{dv}{dy} = 0;\\
&(\sigma We + S)\tau_{11} - 2We\tau_{12} - (4We^2 + 2)i\alpha u - 2We\frac{du}{dy} = 0,\\
&(\sigma We + S)\tau_{12} - We\tau_{22} - Wei\alpha u - \frac{du}{dy} - (2We^2 + 1)i\alpha v - We\frac{dv}{dy} = 0,\\
&(\sigma We + S)\tau_{22} - 2We\frac{du}{dy} - 2\frac{dv}{dy} = 0;\\
&-i\alpha p + \frac{d\tau_{12}}{dy} + i\alpha\tau_{11} = 0, \quad -\frac{dp}{dy} + \frac{d\tau_{22}}{dy} + i\alpha\tau_{12} = 0;
\end{aligned} \tag{3}$$

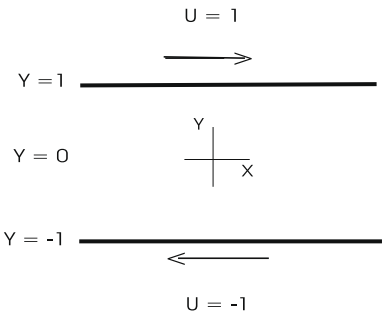

Fig. 1. Configuration of plane Couette flow.

where $S = 1 + i\alpha yWe$ and, at the boundary, $u(y = \pm 1) = 0, v(y = \pm 1) = 0$. The perturbed fields and the growth rate σ of the perturbation are taken as unknowns.

We discretized system (3) by applying Galerkin's weighted residual method. As a first try, we used a common set of basis functions for steady state viscoelastic flows: piecewise quadratic continuous functions to expand the velocity field, piecewise linear continuous functions to expand the stress field and piecewise linear discontinuous functions to expand the pressure field. The computed eigenvalues (evaluated with QZ method) at $We = 10$ and $\alpha = 1$ did not approximate well both the discrete $(-0.056 + \pm i0.950)$ and the continuous part of the spectra (line segment $-0.1 \pm i$), as it is clear in Fig. 2a.

Modifications of system (2) have been proposed in recent years with the goal of stabilizing the numerics to compute steady state flows of viscoelastic liquids. Szady et al. [14] suggest an additional variable $\mathbf{G}$ to represent the velocity gradient as an independent field. For an incompressible liquid, the velocity gradient should be traceless, since $\nabla \cdot \mathbf{v} = 0$. Pasquali and Scriven [15] enforce this by setting

$$\mathbf{G} - \nabla\mathbf{v} + \frac{(\nabla \cdot \mathbf{v})\mathbf{I}}{tr(\mathbf{I})} = \mathbf{0}.$$

The perturbed fields fields, now including the interpolated velocity gradient $\mathbf{G}(\mathbf{x}, t) = \mathbf{G_0}(\mathbf{x}) + \epsilon\mathbf{G}'(y)e^{i\alpha x+\sigma t}$, satisfy

$$\begin{aligned} &\nabla \cdot \mathbf{v} = 0, \quad -\nabla p + \nabla \cdot \boldsymbol{\tau} = 0, \\ &\boldsymbol{\tau} + We\left[\frac{\partial \boldsymbol{\tau}}{\partial t} + (\mathbf{v} \cdot \nabla)\boldsymbol{\tau} - (\mathbf{G})\boldsymbol{\tau} - \boldsymbol{\tau}(\mathbf{G})^T\right] = (\mathbf{G} + \mathbf{G}^{\mathbf{T}}), \\ &\mathbf{G} - \nabla\mathbf{v} + \frac{(\nabla \cdot \mathbf{v})\mathbf{I}}{tr(\mathbf{I})} = 0. \end{aligned} \tag{4}$$

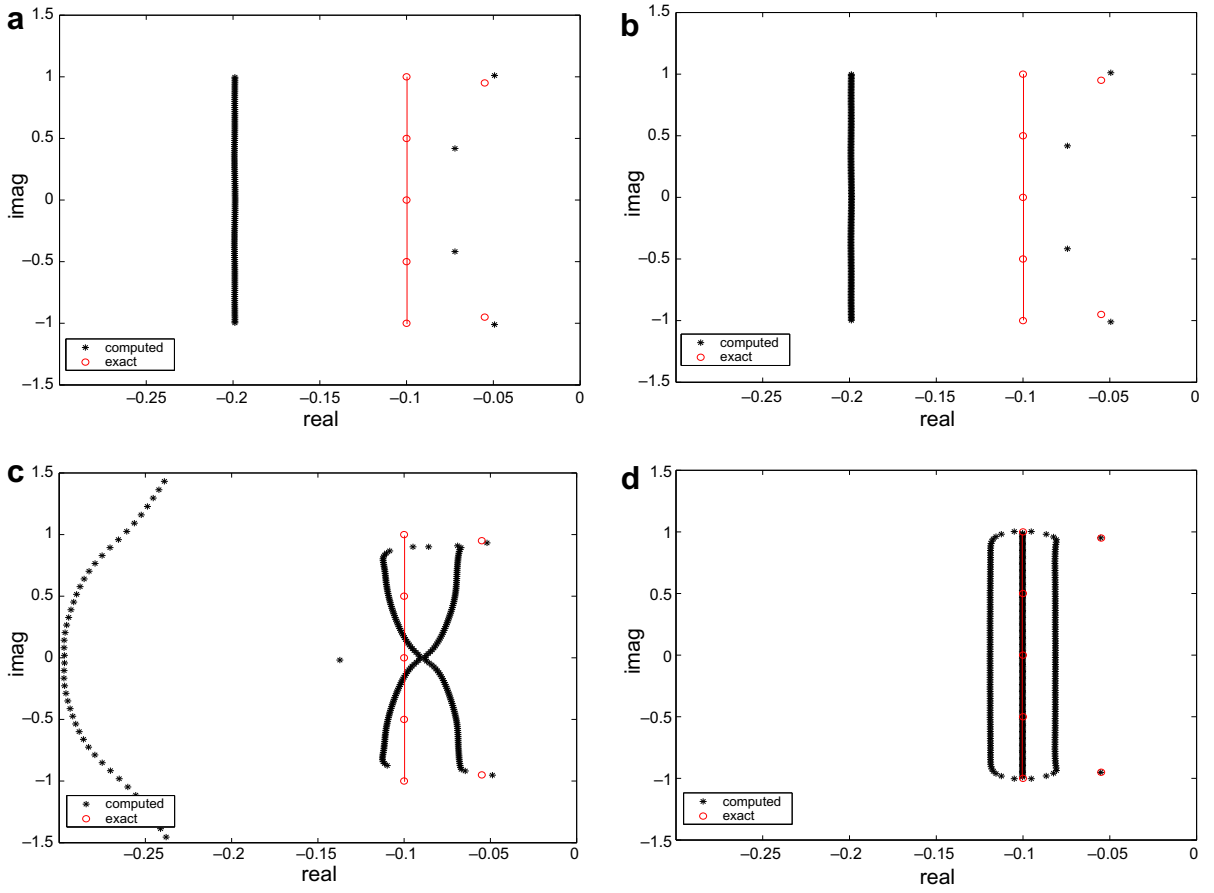

Fig. 2. Computed eigenvalues as a function of the formulations and set of basis functions used: (a) original formulation and continuous linear functions for the stress field; (b) modified formulation and continuous linear functions for the stress and interpolated velocity gradient fields; (c) original formulation and discontinuous linear functions for the stress and interpolated velocity gradient fields; and (d) modified formulation and discontinuous linear functions for the stress and interpolated velocity gradient fields.

As before, we insert in the system above the expressions for the perturbed fields and neglect terms of order $\mathcal{O}(\epsilon^2)$. To simplify notation, we drop primes: the perturbed fields will be represented by $p, \boldsymbol{\tau}$, $\mathbf{v}$ and $\mathbf{G}$. The amplitude of the perturbations and their growth factor satisfy

$$
\begin{aligned}
& i\alpha u + \frac{dv}{dy} = 0; \\
& (\sigma We + S)\tau_{11} - 2We\tau_{12} - (4We^2 + 2)G_{11} - 2WeG_{12} = 0, \\
& (\sigma We + S)\tau_{12} - We\tau_{22} - WeG_{11} - G_{12} - (2We^2 + 1)G_{21} - WeG_{22} = 0, \\
& (\sigma We + S)\tau_{22} - 2WeG_{12} - 2G_{22} = 0; \\
& -i\alpha p + \frac{d\tau_{12}}{dy} + i\alpha\tau_{11} = 0, \quad -\frac{dp}{dy} + \frac{d\tau_{22}}{dy} + i\alpha\tau_{12} = 0; \\
& -\frac{1}{2}i\alpha u + \frac{1}{2}\frac{dv}{dy} + G_{11} = 0, \quad -\frac{du}{dy} + G_{12} = 0, \\
& -i\alpha v + G_{21} = 0, \quad \frac{1}{2}i\alpha u - \frac{1}{2}\frac{dv}{dy} + G_{22} = 0,
\end{aligned}
\tag{5}
$$

where $S = 1 + i\alpha y We$ and, at the boundary, $u(y = \pm 1) = 0, v(y = \pm 1) = 0$.

We expand the unknown fields by the same set of basis functions used before, but now including an expansion for the interpolated velocity gradient field: piecewise quadratic continuous functions to expand the velocity field, piecewise linear continuous functions to expand the stress and velocity gradient fields and piecewise linear discontinuous functions to expand the pressure field. Again, the computed eigenvalues (evaluated with QZ method) did not approximate well both the discrete and the continuous part of the spectra, as it is clear in Fig. 2b.

Realizing that a discontinuous stress field may satisfy the governing equations, we use piecewise linear discontinuous basis functions to expand the stress and velocity gradient fields for both systems of equations (3) and (5), i.e. with and without the interpolated velocity gradient field. The computed eigenvalues are shown in Fig. 2-c-d. The results that approximate well the analytical solution were those obtained with the modified system of equations, where the velocity gradient is treated as an independent field, and linear discontinuous basis functions were used to expand both the stress and velocity gradient fields.

In summary, the weighting functions ϕ_j used for the momentum equations are piecewise Lagrangian quadratic polynomials. For the continuity equation, constitutive equations and interpolated velocity gradient equations, we take piecewise linear discontinuous polynomials χ_j, ψ_j and φ_j. Each perturbed field is approximated by a linear combination of the same basis functions

$$
p_h = \sum_{k=1}^{m} P_k\ \chi_k, \quad \boldsymbol{\tau_h} = \begin{bmatrix} \tau_{11h} & \tau_{12h} \\ \tau_{12h} & \tau_{22h} \end{bmatrix} = \begin{bmatrix} \sum_{k=1}^{m} T_{11k}\psi_k & \sum_{k=1}^{m} T_{12k}\psi_k \\ \sum_{k=1}^{m} T_{12k}\psi_k & \sum_{k=1}^{m} T_{22k}\psi_k \end{bmatrix},
$$

$$
\mathbf{v_h} = \begin{bmatrix} u_h \\ v_h \end{bmatrix} = \begin{bmatrix} \sum_{k=1}^{n} U_k\phi_k \\ \sum_{k=1}^{n} V_k\phi_k \end{bmatrix}, \quad \mathbf{G_h} = \begin{bmatrix} G_{11h} & G_{12h} \\ G_{21h} & G_{22h} \end{bmatrix} = \begin{bmatrix} \sum_{k=1}^{m} \mathcal{G}_{11k}\varphi_k & \sum_{k=1}^{m} \mathcal{G}_{12k}\varphi_k \\ \sum_{k=1}^{m} \mathcal{G}_{12k}\varphi_k & \sum_{k=1}^{m} \mathcal{G}_{22k}\varphi_k \end{bmatrix}.
$$

After integration by parts, the weighted residuals are

$$
R_c^j = \int_{-1}^{1} \left(i\alpha u_h + \frac{dv_h}{dy} \right) \chi_j\ dy;
$$

$$
R_{\tau_{11}}^j = \sigma \int_{-1}^{1} (We\ \tau_{11h})\psi_j\ dy + \int_{-1}^{1} (S\tau_{11h} - 2We\tau_{12h} - (4We^2 + 2)G_{11h} - 2WeG_{12h})\psi_j\ dy;
$$

$$
R_{\tau_{12}}^j = \sigma \int_{-1}^{1} (We\ \tau_{12h})\psi_j\ dy + \int_{-1}^{1} (S\tau_{12h} - We(\tau_{22h} + G_{11h}) - G_{12h} - (2We^2 + 1)G_{21h} - WeG_{22h})\psi_j\ dy;
$$

$$
R_{\tau_{22}}^j = \sigma \int_{-1}^{1} (We\ \tau_{22h})\psi_j\ dy + \int_{-1}^{1} (S\tau_{22h} - 2WeG_{12h} - 2G_{22h})\psi_j\ dy;
$$

$$
R_{mx}^j = \int_{-1}^{1} (i\alpha p_h - i\alpha\tau_{11h})\phi_j\ dy + \int_{-1}^{1} (\tau_{12h})\frac{d\phi_j}{dy}\ dy;
$$

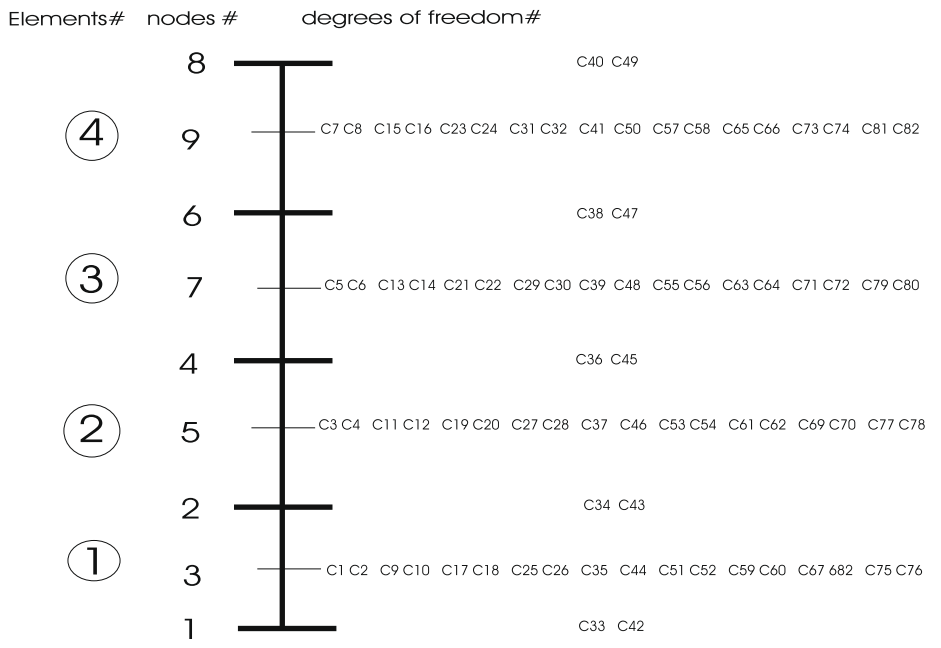

Fig. 3. Numbering scheme for elements, nodes and degrees of freedom for a mesh consisting of four finite elements. The coefficients C1–C8, C9–C32, C33–C50, C51–C82 correspond to pressure, stress tensor, velocity and velocity gradient. The boundary conditions are applied to the velocity degrees of freedom C33, C40, C42, C49.

$$R^j_{my} = \int_{-1}^{1} (i\alpha\tau_{12h})\phi_j \, dy + \int_{-1}^{1} (p_h - \tau_{22h}) \frac{d\phi_j}{dy} \, dy;$$

$$R^j_{G_{11}} = \int_{-1}^{1} \left(-\frac{1}{2} i\alpha u_h + \frac{1}{2} \frac{dv_h}{dy} + G_{11h} \right) \varphi_j \, dy;$$

$$R^j_{G_{12}} = \int_{-1}^{1} \left(-\frac{du_h}{dy} + G_{12h} \right) \varphi_j \, dy, \quad R^j_{G_{21}} = \int_{-1}^{1} (-i\alpha v_h + G_{21h}) \varphi_j \, dy;$$

$$R^j_{G_{22}} = \int_{-1}^{1} \left(\frac{1}{2} i\alpha u_h - \frac{1}{2} \frac{dv_h}{dy} + G_{22h} \right) \varphi_j \, dy.$$

The stress field may be expanded in terms of discontinuous basis function without the need to take into account jumps between elements. In Couette flow, the steady state velocity only varies in the direction perpendicular to the flow and the steady state stress is constant. The $\mathcal{O}(\epsilon)$ terms of the expansion around the steady solution only have derivatives of stress with respect to the y coordinate in the momentum equations (see Eq. (5)), which are eliminated after the integration by parts of the weighted residuals.

The number of algebraic equations is $2n + 8m$, where n is the number of basis functions ϕ_j and m is the number of basis functions of the form ξ_j, ψ_j, φ_j (notice that $\boldsymbol{\tau}$ and $\mathbf{G}$ have respectively 3 and 4 independent entries). For N elements, $n = 2N + 1$ and $m = 2N$, as shown in Fig. 3. Thus, the total number of degrees of freedom of the discretization is $2n + 8m = 20N + 2$.

In vector form, the linear stability problem boils down to solving $\mathbf{R}(\mathbf{c}) = 0$, where the column vector $\mathbf{c}$ consists of the coefficients of the finite element perturbations and $\mathbf{R}$ is the column vector of weighted residual equations:

$$\mathbf{c} = [P_1, \ldots, P_m, T_{11_1}, \ldots, T_{11_m}, T_{12_1}, \ldots, T_{12_m}, T_{22_1}, \ldots, T_{22_m}, U_1, \ldots, U_n, V_1, \ldots, V_n, \mathcal{G}_{11_1}, \ldots, \mathcal{G}_{11_m}, \mathcal{G}_{12_1}, \ldots, \mathcal{G}_{12_m}, \mathcal{G}_{21_1}, \ldots, \mathcal{G}_{21_m}, \mathcal{G}_{22_1}, \ldots, \mathcal{G}_{22_m}]^T,$$

$$\mathbf{R} = [R^1_c, \ldots, R^m_c, R^1_{\tau_{11}}, \ldots, R^m_{\tau_{11}}, R^1_{\tau_{12}}, \ldots, R^m_{\tau_{12}}, R^1_{\tau_{22}}, \ldots, R^m_{\tau_{22}}, R^1_{mx}, \ldots, R^n_{mx}, R^1_{my}, \ldots, R^n_{my}, R^1_{G_{11}}, \ldots, R^m_{G_{11}}, R^1_{G_{12}}, \ldots, R^m_{G_{12}}, R^1_{G_{21}}, \ldots, R^m_{G_{21}}, R^1_{G_{22}}, \ldots, R^m_{G_{22}}]^T.$$

As usual, the sensitivity matrix $\mathbf{A} = \frac{\partial \mathbf{R}}{\partial \mathbf{c}}$ is the linear part of the expansion of $\mathbf{R}$ at $\mathbf{c} = \mathbf{0}$, and we search for vectors $\mathbf{w}$ in its kernel, $\mathbf{A}\mathbf{w} = 0$. Splitting $\mathbf{A}$ according to the growth rate σ, $\mathbf{A} = \mathbf{J} - \sigma\mathbf{M}$, gives rise to the *Jacobian matrix* $\mathbf{J}$ and the *mass matrix* $\mathbf{M}$. We are thus led to the generalized, non-Hermitian eigenproblem (GEVP) $\mathbf{J}\mathbf{c} = \sigma\mathbf{M}\mathbf{c}$, Eq. (1) of the introduction.

Both **M** and **J** partition naturally in a 4×4 block structure with square blocks along the diagonal. Many such blocks are trivially zero. For example, the only non-zero block in the mass matrix **M** is $\mathbf{M_{22}}$, containing the derivatives of the entries $R^j_{\tau_{\ell k}}$ with respect to the variables $\tau^j_{\ell k}$. Keeping track of variable dependencies in a similar fashion, one is led to the configurations below:

$$\mathbf{M} = \left(\begin{array}{c|c|c|c} \mathbf{0} & \mathbf{0} & \mathbf{0} & \mathbf{0} \\ \hline \mathbf{0} & \mathbf{M_{22}} & \mathbf{0} & \mathbf{0} \\ \hline \mathbf{0} & \mathbf{0} & \mathbf{0} & \mathbf{0} \\ \hline \mathbf{0} & \mathbf{0} & \mathbf{0} & \mathbf{0} \end{array}\right) \begin{array}{c} 2N \\ 6N \\ 4N+2 \\ 8N \end{array} \qquad \mathbf{J} = \left(\begin{array}{c|c|c|c} \mathbf{0} & \mathbf{0} & \mathbf{J_{13}} & \mathbf{0} \\ \hline \mathbf{0} & \mathbf{J_{22}} & \mathbf{0} & \mathbf{J_{24}} \\ \hline \mathbf{J_{31}} & \mathbf{J_{32}} & \mathbf{0} & \mathbf{0} \\ \hline \mathbf{0} & \mathbf{0} & \mathbf{J_{43}} & \mathbf{J_{44}} \end{array}\right) \begin{array}{c} 2N \\ 6N \\ 4N+2 \\ 8N \end{array} \tag{6}$$

The polynomial associated to the GEVP (1), then, is of degree at most 6*N*, a number much smaller than $20N + 2$, the dimension of the full matrix **A**. The $14N + 2$ missing dimensions are related to the *eigenvalues at infinity*. Indeed, in a nutshell, perturbations of the mass matrix, e.g. $\mathbf{M}^* = \mathbf{M} + \epsilon$, have large eigenvalues in the spectrum, which go to infinity as ϵ goes to 0. Truncation errors in the numerical methods used to calculate the spectrum of the GEVP give rise to perturbations of the mass matrix and lead to the appearance of very large eigenvalues. With the method of the following section, we count the eigenvalues at infinity correctly (there are many more), and, by eliminating them, we may transform the GEVP into a smaller, non-degenerate one.

It is important to note that the method that is presented next can be applied on the formulation with or without the interpolated velocity gradient field. However, the matrices transformations will not be exactly the same because they depend on the structure of the matrices involved, which is a direct function of the relationship between equations and variables.

Moreover, the fact that the problem used here to test the procedure is a unidirectional Couette flow does not bring any particularity to the matrices' structure, which would be very similar for a two-dimensional creeping flow. The only difference is the size and structure of each individual block, which is a function of the finite element mesh and basis functions used to expand each field. Consequently, the method presented in the following section can be used with different sets of basis functions and can be easily generalized to two-dimensional flows. We presented for the particular case of a Couette flow of an UCM liquid to make the matrix transformations used more clear and to be able to compare the computed spectrum to those presented in the literature.

3. Getting rid of eigenvalues at infinity

Valerio et al. [13] showed that the GEVP resulting from linear stability analysis of viscous flow may be reduced, by a sequence of operations in the spirit of a partial Gaussian elimination, to a smaller GEVP with spectrum equal to the finite portion of the spectrum of the original GEVP. The approach was used to compute the spectrum of the Couette flow of a Newtonian liquid at moderate Reynolds number, leading to sparse matrices three times smaller, and numerical algorithms with a speed-up factor of 35. In this section, we show that a similar approach can be used for viscoelastic flows, with even larger gains.

The (generalized) eigenvalues σ of the GEVP represented in Eq. (1) are the roots of the characteristic polynomial $p(\sigma) \equiv \det(\mathbf{A}) \equiv \det(\mathbf{J} - \sigma\mathbf{M})$. Said differently, we are interested in the values of σ for which the homogeneous system $(\mathbf{J} - \sigma\mathbf{M})\mathbf{c} = 0$ has a non-trivial solution. Thus, if one replaces both **J** and **M** by matrices $\widetilde{\mathbf{J}}$ and $\widetilde{\mathbf{M}}$, the GEVP's $\mathbf{Jc} = \sigma\mathbf{Mc}$ and $\widetilde{\mathbf{J}}\tilde{\mathbf{c}} = \sigma\widetilde{\mathbf{M}}\tilde{\mathbf{c}}$ have the same eigenvalues if the homogeneous systems $(\widetilde{\mathbf{J}} - \sigma\widetilde{\mathbf{M}})\tilde{\mathbf{c}} = 0$ and $(\mathbf{J} - \sigma\mathbf{M})\mathbf{c} = 0$ have a non-trivial solution for the same values of σ. More concretely, consider multiplications $\widetilde{\mathbf{J}} = \mathbf{XJY}$ and $\widetilde{\mathbf{M}} = \mathbf{XMY}$ of both **J** and **M** by invertible matrices **X** and **Y** independent of σ. The matrices **X** and **Y** might arise while solving the homogeneous system $(\mathbf{J} - \sigma\mathbf{M})\mathbf{c} = 0$ with a two-sided Gaussian elimination, in the sense that row and column elementary operations are allowed. Clearly, the solutions of the systems $(\widetilde{\mathbf{J}} - \sigma\widetilde{\mathbf{M}})\tilde{\mathbf{c}} = 0$ and $(\mathbf{J} - \sigma\mathbf{M})\mathbf{c} = 0$ are related by $\mathbf{Y}\tilde{\mathbf{c}} = \mathbf{c}$, so it is algebraically simple to translate between (generalized) eigenvectors of both problems.

The matrix structure is of essence here, and an example with only $N = 4$ finite elements is shown in Fig. 4: the labelling of entries follows Fig. 3. In this case, there are $20N + 2 = 82$ degrees of freedom. The equations associated to the Dirichlet boundary conditions correspond to rows 33, 40, 42 and 49. By inspection, on each such row, the only non-zero entry is the diagonal position, equal to 1. Thus, without changes in the polynomial $p(\sigma)$, one may remove four rows and columns of **A**, obtaining the matrix $\mathbf{A_b} = (\mathbf{J_b} - \sigma\mathbf{M_b})$, which in general is of dimension $20N - 2$.

We repartition $\mathbf{A_b}$, by fitting into the same block the first two blocks of rows and columns. For the new partition, shown in Eq. (7), $\mathbf{A_{11b}}$ and $\mathbf{A_{33b}}$ are squares of the same dimension 8*N*

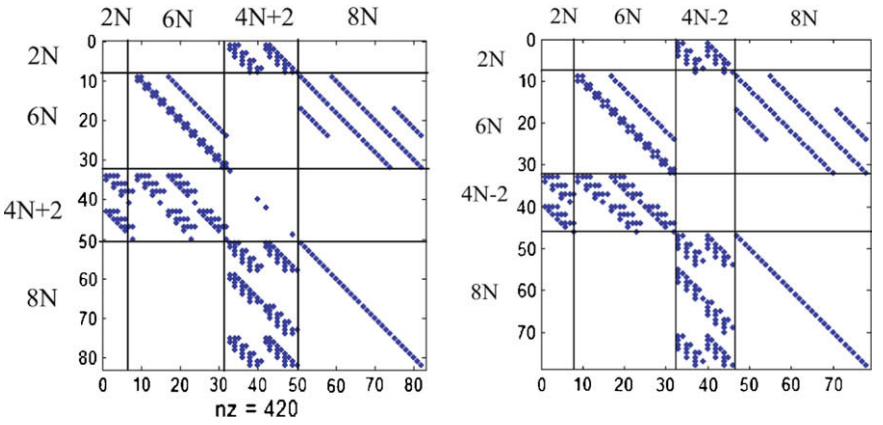

Fig. 4. Left: the non-zero entries of **A**, $N = 4$. Right: $\mathbf{A_b}$, obtained by removing 4 rows and columns of **A**.

$$\mathbf{A}_{\mathrm{b}} = \left(\begin{array}{c|c|c} \mathbf{A}_{11\mathrm{b}}(\sigma) & \mathbf{A}_{12\mathrm{b}} & \mathbf{A}_{13\mathrm{b}} \\ \hline \mathbf{A}_{21\mathrm{b}} & \mathbf{0} & \mathbf{0} \\ \hline \mathbf{0} & \mathbf{A}_{32\mathrm{b}} & \mathbf{A}_{33\mathrm{b}} = \mathbf{D} \end{array}\right) \begin{array}{c} 8N \\ \hline 4N-2 \\ \hline 8N \end{array} \qquad (7)$$

$$\begin{array}{ccc} 8N & 4N-2 & 8N \end{array}$$

On $\mathbf{A_b}$, only the block $\mathbf{A_{11b}}$ has any contribution from the mass matrix and consequently depends on the growth factor σ and on the Wessenberg number *We*. The Jacobian matrix **J** and $\mathbf{J_b}$ are simultaneously invertible or not, and invertibility happens generically. It breaks down at *turning points* of the solution path constructed along increasing *We*. In other words, for a given flow there are isolated values of *We* at which **J** (or $\mathbf{J_b}$) may become singular. The triple ($\mathbf{0}$ $\mathbf{A_{32b}}$ $\mathbf{D}$) is formed by the last $8N$ rows of $\mathbf{J_b}$ and does not depend on *We*. These rows are always linearly independent, otherwise the square matrix $\mathbf{J_b}$ would have been singular for all values of *We*. Thus, either the submatrix **D** is invertible or there must be a permutation of the last $12N-2$ columns of $\mathbf{J_b}$ for which the bottom $8N \times 8N$ block is invertible. For the Couette flow of the UCM liquid, **D** is (invertible) diagonal. Thus, the block $\mathbf{A_{32b}}$ can be eliminated by performing elementary operations on columns, yielding $\widetilde{\mathbf{A}}$:

$$\tilde{\mathbf{A}} = \left(\begin{array}{c|c|c} \mathbf{A}_{11\mathrm{b}}(\sigma) & \tilde{\mathbf{A}}_{12} & \mathbf{A}_{13\mathrm{b}} \\ \hline \mathbf{A}_{21\mathrm{b}} & \mathbf{0} & \mathbf{0} \\ \hline \mathbf{0} & \mathbf{0} & \mathbf{D} \end{array}\right) = \mathbf{A}_{\mathrm{b}}\,\mathbf{T}_{\mathrm{r}}, \text{ where } \mathbf{T}_{\mathrm{r}} = \left(\begin{array}{c|c|c} \mathbf{I}_{[8N]} & \mathbf{0} & \mathbf{0} \\ \hline \mathbf{0} & \mathbf{I}_{[4N-2]} & \mathbf{0} \\ \hline \mathbf{0} & -\mathbf{D}^{-1}\mathbf{A}_{32\mathrm{b}} & \mathbf{I}_{[8N]} \end{array}\right).$$

The modified block is evaluated as $\widetilde{\mathbf{A}}_{12} = \mathbf{A_{12b}} - \mathbf{A_{13b}}\mathbf{D}^{-1}\mathbf{A_{32b}}$.

The characteristic polynomial $p_1(\sigma)$ of $\widetilde{\mathbf{A}}$ is

$$p_1(\sigma) = \det(\widetilde{\mathbf{A}}) = \det(\mathbf{A_b})\det(\mathbf{T_r}) = \det(\mathbf{A_b}) = p(\sigma).$$

Again, $\widetilde{\mathbf{A}}$ and $\mathbf{A_b}$ have the same eigenvalues. Now, making use of the special form of $\widetilde{\mathbf{A}}$, write $p_1(\sigma) = \det(\widetilde{\mathbf{A}}) = \det(\mathbf{D})\det(\mathbf{B}_{\widetilde{\mathbf{A}}}) = \kappa_1 p_2(\sigma)$, where **D** is an invertible diagonal matrix independent of σ, $\mathbf{B}_{\widetilde{\mathbf{A}}}$ is the 2×2 top block submatrix of $\widetilde{\mathbf{A}}$ and $p_2(\sigma) = \det(\mathbf{B}_{\widetilde{\mathbf{A}}})$. Thus, the eigenvalues of $\mathbf{B}_{\widetilde{\mathbf{A}}}$ are the same as the finite eigenvalues of $\mathbf{A_b}$. For $N = 4$, $\widetilde{\mathbf{A}}$ is shown in Fig. 5.

We consider a final partition of $\mathbf{B}_{\widetilde{\mathbf{A}}}$, shown below. This time, we mix variables pertaining to different fields. We now use corner square blocks (independent of σ) to perform elementary operations. The case $N = 4$ is displayed on the right side of Fig. 5. The argument which showed that the Jacobian matrix is generally non-singular implies also that the $4N-2$ rows and columns of the triples $(\mathbf{B}_{\widetilde{\mathbf{A}}_{31}}, \mathbf{B}_{\widetilde{\mathbf{A}}_{32}}, \mathbf{0})$ and $(\mathbf{B}_{\widetilde{\mathbf{A}}_{13}}, \mathbf{B}_{\widetilde{\mathbf{A}}_{23}}, \mathbf{0})^{\mathbf{T}}$ are linearly independent. Again, there are permutations on the last rows and columns that give rise to invertible corner blocks: for the Couette flow no permutations are necessary

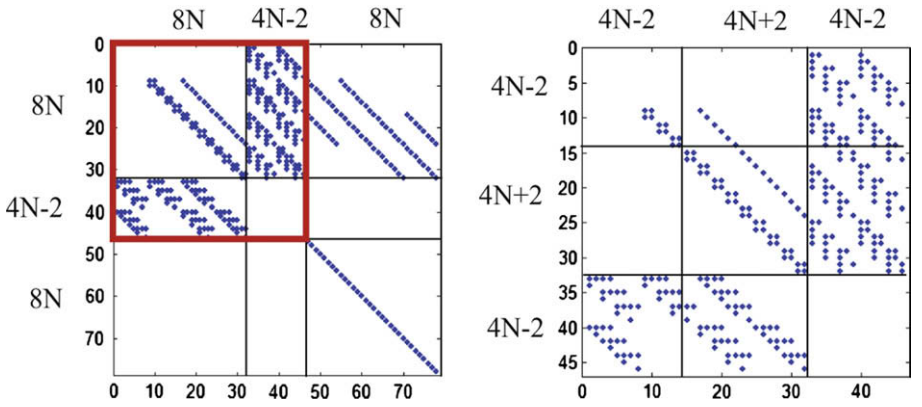

Fig. 5. $\tilde{\mathbf{A}} = \mathbf{A_b T_r}$ and $\mathbf{B}_{\tilde{\mathbf{A}}}$ appropriately partitioned, $N = 4$.

$$\mathbf{B}_{\tilde{\mathbf{A}}} = \left(\begin{array}{c|c|c} \mathbf{B}_{\tilde{\mathbf{A}}11}(\sigma) & \mathbf{B}_{\tilde{\mathbf{A}}12}(\sigma) & \mathbf{B}_{\tilde{\mathbf{A}}13} \\ \hline \mathbf{B}_{\tilde{\mathbf{A}}21}(\sigma) & \mathbf{B}_{\tilde{\mathbf{A}}22}(\sigma) & \mathbf{B}_{\tilde{\mathbf{A}}23} \\ \hline \mathbf{B}_{\tilde{\mathbf{A}}31} & \mathbf{B}_{\tilde{\mathbf{A}}32} & \mathbf{B}_{\tilde{\mathbf{A}}33} = \mathbf{0} \end{array}\right) \begin{array}{l} 4N-2 \\ 4N+2, \\ 4N-2 \end{array} \qquad \mathbf{b} = \begin{pmatrix} \mathbf{b}_1 \\ \mathbf{b}_2 \\ \mathbf{b}_3 \end{pmatrix}$$

$$4N-2 \quad 4N+2 \quad 4N-2$$

The next step should be clear: set

$$\widetilde{\mathbf{B}_{\tilde{\mathbf{A}}}} = \left(\begin{array}{c|c|c} \mathbf{B}_{\tilde{\mathbf{A}}11}(\sigma) & \widetilde{\mathbf{B}_{\tilde{\mathbf{A}}12}}(\sigma) & \mathbf{B}_{\tilde{\mathbf{A}}13} \\ \hline \widetilde{\mathbf{B}_{\tilde{\mathbf{A}}21}}(\sigma) & \widetilde{\mathbf{B}_{\tilde{\mathbf{A}}22}}(\sigma) & \mathbf{0} \\ \hline \mathbf{B}_{\tilde{\mathbf{A}}31} & \mathbf{0} & \mathbf{0} \end{array}\right) = \mathbf{F}_\ell \, \mathbf{B}_{\tilde{\mathbf{A}}} \, \mathbf{F}_r,$$

where $\mathbf{F}_\ell$ and $\mathbf{F}_r$ are block elementary matrices. Both are partitioned like $\mathbf{B}_{\tilde{\mathbf{A}}}$, with identity blocks along the diagonal and each one has a unique off-diagonal non-zero block: for $\mathbf{F}_\ell$, its (21) block equals $-\mathbf{B}_{\tilde{\mathbf{A}}_{23}} \mathbf{B}^{-1}_{\tilde{\mathbf{A}}_{13}}$ and for $\mathbf{F_r}$, its (12) block is $-\mathbf{B}^{-1}_{\tilde{\mathbf{A}}_{31}} \mathbf{B}_{\tilde{\mathbf{A}}_{32}}$. As explained bellow, the only block needed to compute the finite eigenvalues is the central block $\widetilde{\mathbf{B}_{\tilde{\mathbf{A}}_{22}}}$. It is computed as

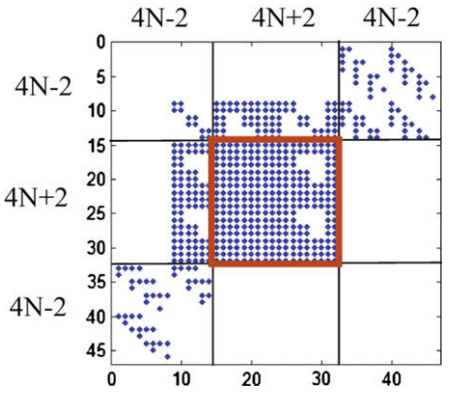

Fig. 6. The matrix $\widetilde{\mathbf{B}_{\tilde{\mathbf{A}}}} = \mathbf{F}_\ell \mathbf{B}_{\tilde{\mathbf{A}}} \mathbf{F}_r$, $N = 4$.

$$\widetilde{\mathbf{B}}_{\mathbf{A}_{22}} = -\mathbf{B}_{\mathbf{A}_{23}}\mathbf{B}_{\mathbf{A}_{13}}^{-1}(-\mathbf{B}_{\mathbf{A}_{11}}\mathbf{B}_{\mathbf{A}_{31}}^{-1}\mathbf{B}_{\mathbf{A}_{32}} + \mathbf{B}_{\mathbf{A}_{12}}) - \mathbf{B}_{\mathbf{A}_{21}}\mathbf{B}_{\mathbf{A}_{31}}^{-1}\mathbf{B}_{\mathbf{A}_{32}} + \mathbf{B}_{\mathbf{A}_{22}}.$$

The structure of the matrix $\widetilde{\mathbf{B}}_{\mathbf{A}}$ is shown in Fig. 6 for $N = 4$. The central block, $\widetilde{\mathbf{B}}_{\mathbf{A}_{22}}$ is a very sparse matrix for large N.

For $p_3(\sigma) = \det(\widetilde{\mathbf{B}}_{\mathbf{A}})$ we still have $p_3(\sigma) = p_2(\sigma) = \det(\mathbf{B}_{\mathbf{A}})$, but more is true, since $\widetilde{\mathbf{B}}_{\mathbf{A}}$ is non-singular, the blocks $\mathbf{B}_{\mathbf{A}_{13}}$ and $\mathbf{B}_{\mathbf{A}_{31}}$ are invertible matrices independent of σ : $p_3(\sigma)$ and $\det(\widetilde{\mathbf{B}}_{\mathbf{A}_{22}}(\sigma))$ have the same finite roots, which are the same as the finite roots of $p(\sigma)$, the generalized eigenvalues of the original stability problem.

Now, generically, $\det(\widetilde{\mathbf{B}}_{\mathbf{A}_{22}}(\sigma))$ is of degree $4N + 2$, the dimension of the block $\widetilde{\mathbf{B}}_{\mathbf{A}_{22}}(\sigma)$: the original GEVP of dimension $20N + 2$ has been reduced to a GEVP of dimension $4N + 2$, $(\widetilde{\mathbf{J}}_{\mathbf{A}_{22}} - \sigma\widetilde{\mathbf{M}}_{\mathbf{A}_{22}})\mathbf{d} = \mathbf{0}$, where the matrix $\widetilde{\mathbf{M}}_{\mathbf{A}_{22}}$ is (generically) invertible: all the eigenvalues are now finite. In principle, the problem may be reduced to a standard eigenvalue problem and the complete physically relevant spectrum can be evaluated by solving a regular GEVP that is approximately 1/5 of the size of the original GEVP.

We now keep track of the transformations induced on the generalized eigenvectors by the operations above. Start with a vector $\mathbf{c}$ satisfying $\mathbf{Ac} = \mathbf{0}$ associated to a generalized eigenvalue σ. The solution $\mathbf{c_b}$ of the system $\mathbf{A_b c_b} = \mathbf{0}$ (for the same σ) is obtained from $\mathbf{c}$ by removing the four coordinates equal to 0 at the entries related to the Dirichlet boundary conditions. The solution of $\widetilde{\mathbf{A}}\tilde{\mathbf{c}} = \mathbf{0}$ solves $\mathbf{T_r}\tilde{\mathbf{c}} = \mathbf{c_b}$, and the inverse of $\mathbf{T_r}$ differs from $\mathbf{T_r}$ by an overall change of sign in the (3,2)-block.

We now relate the non-trivial solutions of $\mathbf{B}_{\mathbf{A}}\mathbf{b} = \mathbf{0}$ to $\tilde{\mathbf{c}} = (\tilde{\mathbf{c}}_1, \tilde{\mathbf{c}}_2, \tilde{\mathbf{c}}_3)^{\mathbf{t}}$. Here, $\tilde{\mathbf{c}}$ is partitioned in accordance to the block structure of $\widetilde{\mathbf{A}}$. The system $\widetilde{\mathbf{A}}\tilde{\mathbf{c}} = \mathbf{0}$ gives

$$\widetilde{\mathbf{A}}_{11}\tilde{\mathbf{c}}_1 + \widetilde{\mathbf{A}}_{12}\tilde{\mathbf{c}}_2 + \widetilde{\mathbf{A}}_{13}\tilde{\mathbf{c}}_3 = \mathbf{0}, \quad \widetilde{\mathbf{A}}_{21}\tilde{\mathbf{c}}_1 = \mathbf{0}, \quad \mathbf{D}\tilde{\mathbf{c}}_3 = \mathbf{0}.$$

Since $\mathbf{D}$ is invertible, $\tilde{\mathbf{c}}_3 = \mathbf{0}$. The first equations then imply $\mathbf{b} = (\tilde{\mathbf{c}}_1, \tilde{\mathbf{c}}_2)^{\mathbf{t}}$.

Use $\widetilde{\mathbf{B}}_{\mathbf{A}} = \mathbf{F}_\ell\mathbf{B}_{\mathbf{A}}\mathbf{F}_r$ and the assumption that $\mathbf{F}_\ell$ is invertible to conclude that the solution $\tilde{\mathbf{b}}$ of $\widetilde{\mathbf{B}}_{\mathbf{A}}\tilde{\mathbf{b}} = \mathbf{0}$ satisfies $\mathbf{F}_r\tilde{\mathbf{b}} = \mathbf{b}$. We are left with relating $\tilde{\mathbf{b}}$ with the solution $\mathbf{d}$ of $\widetilde{\mathbf{B}}_{\mathbf{A}_{22}}\mathbf{d} = \mathbf{0}$. Now, partition $\tilde{\mathbf{b}} = (\tilde{\mathbf{b}}_1, \tilde{\mathbf{b}}_2, \tilde{\mathbf{b}}_3)^t$ and write $\widetilde{\mathbf{B}}_{\mathbf{A}}\tilde{\mathbf{b}} = \mathbf{0}$ in block form. Assuming the invertibility of $\mathbf{B}_{\mathbf{A}_{31}}$ and $\mathbf{B}_{\mathbf{A}_{13}}$, it is easy to see, sequentially, that $\tilde{\mathbf{b}}_1 = \mathbf{0}, \tilde{\mathbf{b}}_2$ is an eigenvector of $\widetilde{\mathbf{B}}_{\mathbf{A}_{22}}$ (and hence, generically, one may take without loss $\tilde{\mathbf{b}}_2 = \mathbf{d}$) and finally $\tilde{\mathbf{b}}_3 = -\mathbf{B}_{\mathbf{A}_{13}}^{-1}\widetilde{\mathbf{B}}_{\mathbf{A}_{12}}\mathbf{d}$. The upshot is that from the eigenvector $\mathbf{d}$ of the reduced GEVP one may retrieve the eigenvector related to the same σ of the original stability problem.

4. Numerical results

We compare the results obtained with our method with data available in the literature. The calculations were performed using $We = 10$ and $\alpha = 1$, the same parameters used by Sureshkumar [9].

First, we perform an internal validation. The results of the LAPACK routine ZGEEV for the reduced and the original GEVP on a mesh of $N = 60$ elements essentially agreed to full numerical precision (eight digits). Indeed, there are no approximations in the reduced problem: it only takes advantage of the structure of the matrices. The dimensions of the original eigenproblem is $20N + 2 = 1202$. The reduced matrix, instead, has dimension $4N + 2 = 242$: this is general – dimensions are in the proportion of 5 to 1. For eigenvectors, the agreement is also excellent.

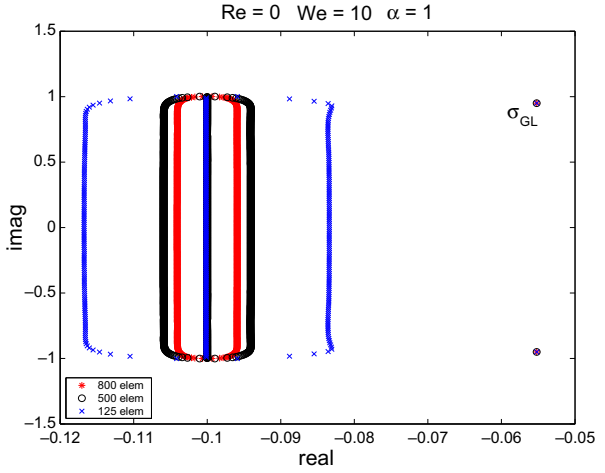

Fig. 7. Spectrum of plane Couette flow UCM liquid with $We = 10$ and $\alpha = 1$, for $N = 125$, 500 and 800 elements.

Table 1
CPU time in seconds, for the original and reduced GEVP's.

N	$20N+2$	$4N+2$	t_{orig}	t_{red}	t_{orig}/t_{red}
60	1202	242	140	3.1	45
100	2002	402	629	13	48
125	2502	502	1252	21	59
150	3002	602	–	43.6	–
200	4002	802	–	85.8	–
300	6002	1202	–	254.3	–

The approximate spectrum obtained by the Galerkin discretization is shown in Fig. 7 for three different meshes with $N = 125$, 500 and 800 elements. It contains the two Gorodstov-Leonov modes and a set of eigenvalues approximating the continuous part of the true spectrum. The computed GL modes are essentially the same starting from $N = 125$ elements:

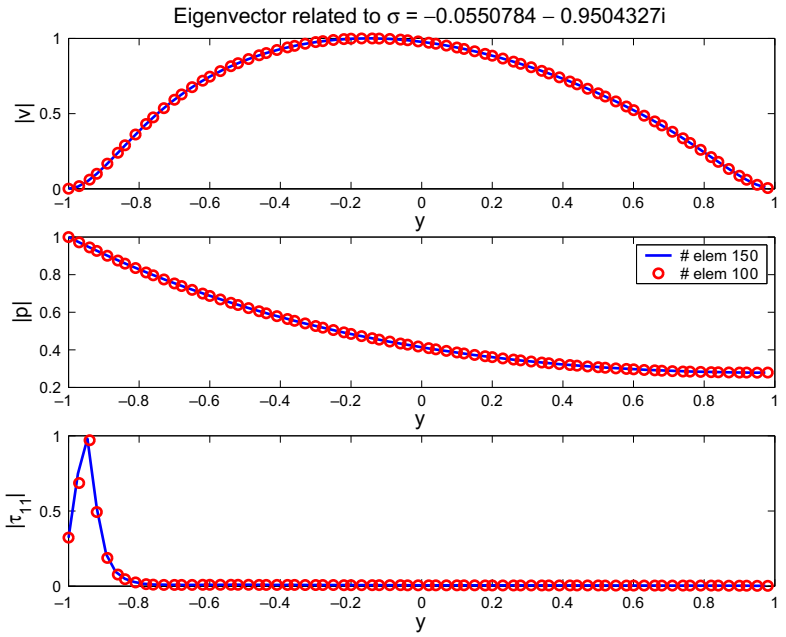

Fig. 8. Modulus of the transversal velocity, pressure and normal component of the stress tensor along the flow direction related to the bottom GL-mode $\sigma_{GL} = -0.0550784 - 0.9504327i$.

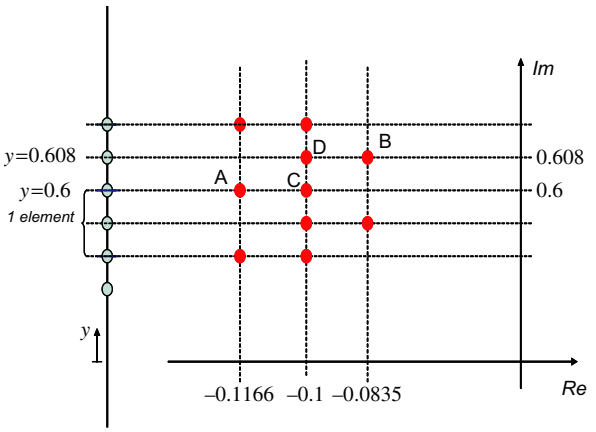

Fig. 9. Detail of the spectrum near $-0.1 + 0.6i$ at $We = 10, \alpha = 1$ and $N = 125$.

the relative deviation comparing results for $N = 125$ and $N = 500$ is 10^{-6}. The values agree well with those obtained by Sureshkumar [9] using streamfunction formulation and a spectral method.

As in the spectral method predictions of Sureshkumar [9] and Wilson et al. [4], the approximation of the continuous spectrum is not precise: for each fixed choice of N, we identified what looks like three lines of eigenvalues close to the continuous spectrum. One such line – not located in the quoted references – lie near the spectrum related to the known analytical solution, the line segment $-1/We \pm i\alpha = -0.1 \pm i$. The computed eigenvalues approximating this segment have their real part equal to $-1/We = -0.1$ with an error of $\pm 10^{-7}$. The imaginary parts are uniformly distributed from -0.99853 to 0.99853. The number of such eigenvalues is equal to $2N - 1$. The other two lines of eigenvalues form an oval around the analytical solution and are similar to those identified by [9,4]. As in [9,4], the oval slowly converges to the analytical solution. With 800 elements, the relative error of the approximations to the continuous part of the spectrum is less than 4%.

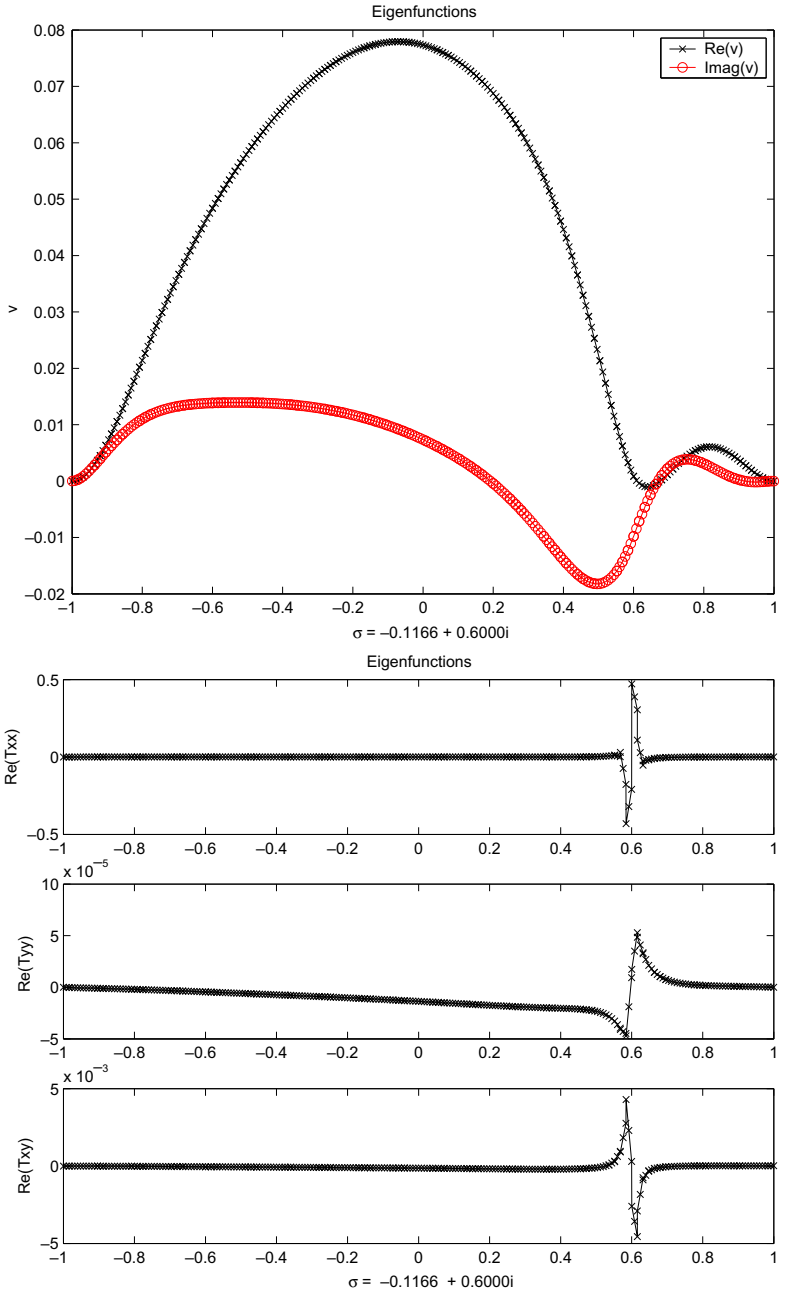

Fig. 10. Eigenfunctions associated with eigenvalue A, indicated in Fig. 9: (a) vertical velocity and (b) stress components.

For different values of N, Table 1 gives the CPU time required to solve both the original and the reduced GEVP's. The latter includes the time required to obtain the reduced GEVP. The speed-up factor is approximately equal to 50. For $N \geqslant 150$, software memory was not enough to solve the original GEVP.

Eigenvectors have coordinates of three different natures: velocity, pressure and stress. The eigenvector of the bottom GL mode is shown in Fig. 8. The absolute values of the transversal velocity and pressure are smooth, whereas the absolute value of the $(1,1)$ entry of the stress tensor field presents a peak, with location dependent on the imaginary part of the GL mode.

We now focus on the continuous part of the spectrum, the interval of eigenvalues with real part $-1/We = -0.1$. Our numerical results indicate that each eigenvalue in the interval gives rise to two eigenvalues of the discrete problem, one with the same real part -0.1 and the other oscillating from right to left, according to parity. Fig. 9 sketches the discrete eigenvalues near $-0.1 + 0.6i$ for $N = 125$. The number of eigenvalues with real part less than -0.1 is equal to the number of nodes located on element boundaries. The imaginary part of each such eigenvalue is in good agreement with a node coordinate.

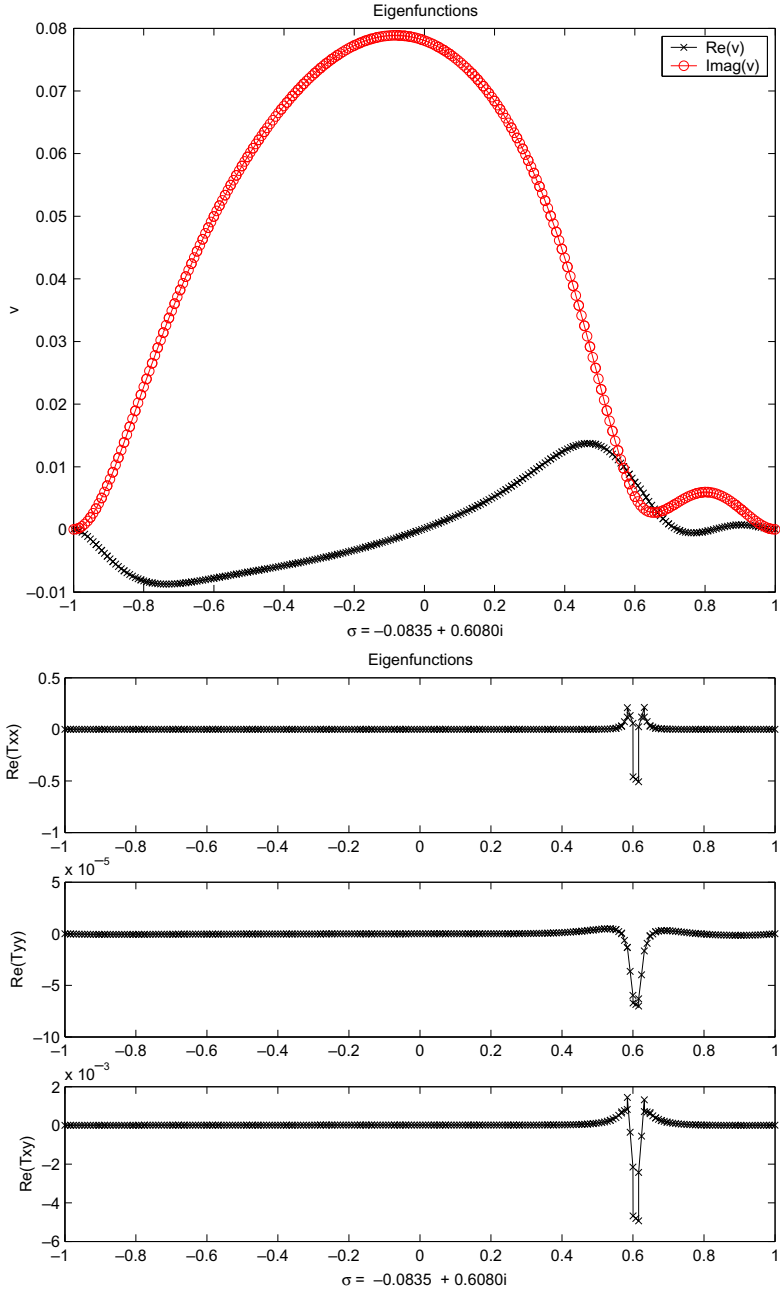

Fig. 11. Eigenfunctions associated with eigenvalue B, indicated in Fig. 9: (a) vertical velocity and (b) stress components.

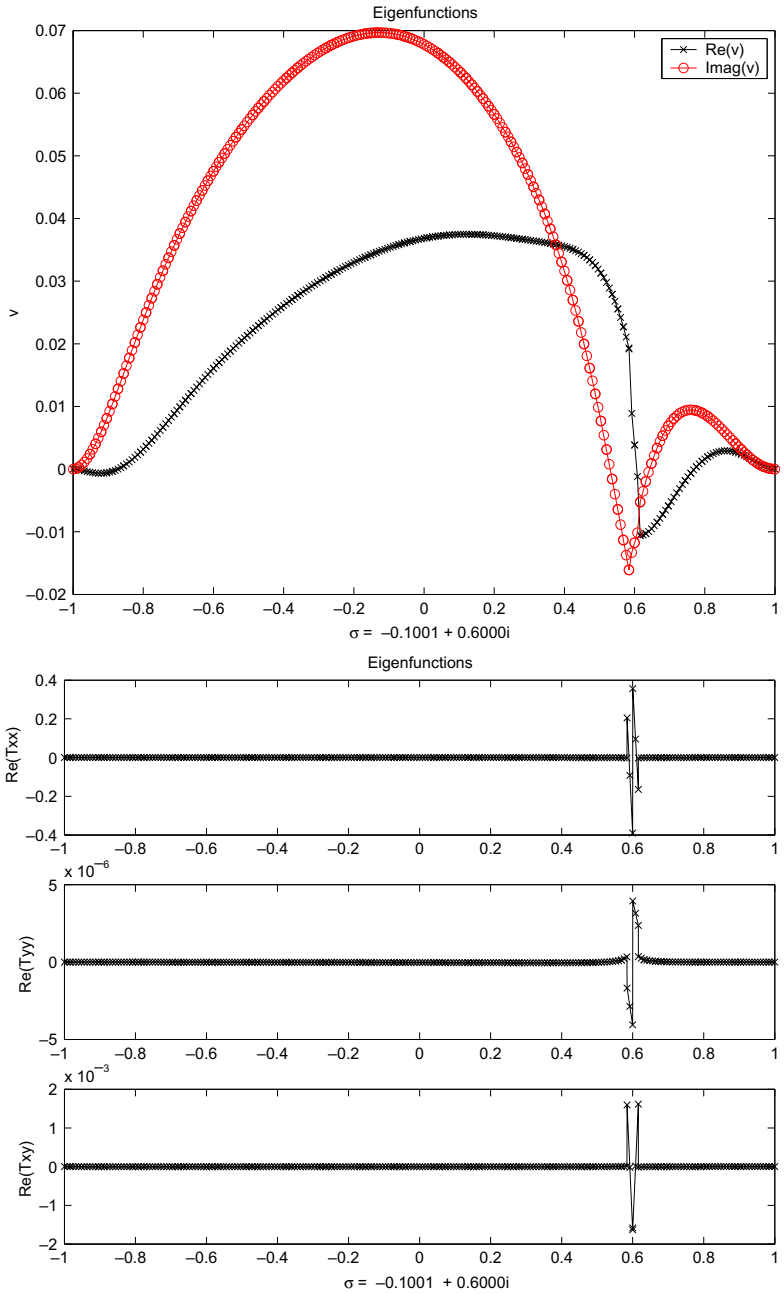

Fig. 12. Eigenfunctions associated with eigenvalue C, indicated in Fig. 9: (a) vertical velocity and (b) stress components.

Similarly, the number of eigenvalues with real part equal to -0.1 equals the number of nodes of the mesh and the imaginary part of each eigenvalue is close to the coordinate of one such node. Finally, there are as many eigenvalues with real part greater than -0.1 as elements, and its imaginary parts agree with the coordinate of the middle node of each element.

The eigenfunctions associated with the eigenvalues marked as A and B in Fig. 9 are presented in Figs. 10 and 11. The vertical velocity and stress fields behave like the analytical solution obtained by Graham [10]. More precisely, Graham's analytic solutions provide a two-dimensional subspace of eigenfunctions for each point in the continuous spectrum: our computations obtain approximations of elements in these subspaces. All the stress components are singular at $y = 0.6$. Also, as observed by Graham, the computed stress components are such that $|T_{xx}| \gg |T_{xy}| \gg |T_{yy}|$ and the region around $y = 0.6$ affected by the singular behavior is larger for the T_{yy} field. Both observations are consistent with the analytical singularity strength of each stress component.

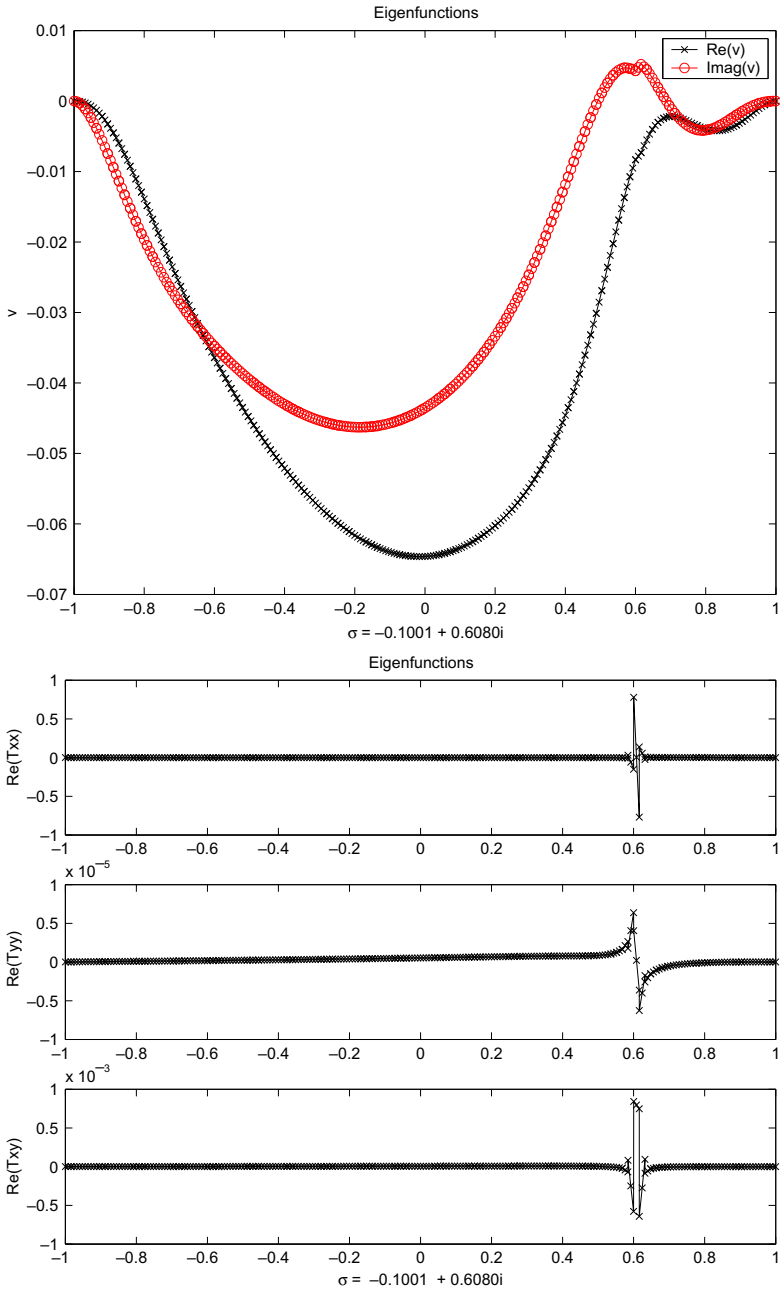

Fig. 13. Eigenfunctions associated with eigenvalue D, indicated in Fig. 9: (a) vertical velocity and (b) stress components.

The eigenfunctions associated with the eigenvalues C and D in Fig. 9 are presented in Figs.12 and 13. The corresponding eigenfunctions are not as smooth as those associated with eigenvalues A and B. Both velocity and stress fields are jagged around the singular point. Again, there is good agreement between the computed eigenfunctions and Graham's results.

Our numerics did not identify eigenfunctions of the type obtained analytically by Kupferman [11]: in that case, velocity components are identically zero and stress components consist of deltas, and its first and second derivatives.

5. Final remarks

This work presents a finite element formulation for the problem of linear stability analysis of a plane Couette flow of an UCM liquid. The computed eigenspectrum provides a better approximation of the continuous part of the spectrum than the

available computations making use of the streamfunction formulation and spectral methods. The computed eigenfunctions approximate well the analytical solutions derived by Graham [10].

The stability problem reduces to the solution of a generalized eigenvalue problem. We introduce a method to eliminate all the eigenvalues at infinity. The algorithm gives rise to an equivalent reduced GEVP with non-singular matrices, whose dimension is approximately $1/5$ of the original one. The finite part of the spectrum of both GEVP's is equal. The main advantages of the new method are

- Eigenvalues at infinity are eliminated without either mapping or preconditioning techniques, which are computationally expensive.
- Without performing approximations, the dimension of the eingenproblem is divided by five.
- The reduced GEVP is non-singular and sparse and may be rewritten as a genuine EVP.

Such features decrease significantly the computational cost of the evaluation of the eigenspectrum of an incompressible viscoelastic flow. In the example presented, the method was 50 times faster than the numerical solution of the original GEVP. The method takes advantage of the structure of the matrices, which is a function of the relationship between governing equations and variables, and it is completely independent of the discretization method. The fact that the problem used as a test here is a unidirectional flow does not bring any particularity to the structure of the Jacobian and Mass matrices, which would be very similar for a two-dimensional flow.

Acknowledgements

J.V. Valério, C. Tomei acknowledge grants from FAPERJ. The three authors acknowledge grants from CNPq. J.V. Valério is grateful to L.E. Scriven and J.M. de Santos for discussions and encouragement during her stay at the University of Minnesota, partially subsidized by CAPES.

References

[1] V.A. Gorodtsov, A.I. Leonov, On a linear instability of plane Couette flow of viscoelastic fluid, J. Appl. Math. Mech. 31 (1967) 310.
[2] M. Renardy, Y. Renardy, Linear stability of plane Couette flow of an upper convected Maxwell fluid, J. Non-Newtonian Fluid Mech. 22 (1996) 23.
[3] R. Sureshkumar, A.N. Beris, Linear stability analysis of viscoelastic Poiseuille flow using an Arnoldi-based orthogonalization algorithm, J. Non-Newtonian Fluid Mech. 56 (1995) 151.
[4] H.J. Wilson, M. Renardy, Y. Renardy, Structure of the spectrum in zero Reynolds numbers in shear flow of UCM and Oldroyd-B liquids, J. Non-Newtonian Fluid Mech. 80 (1999) 251.
[5] R. Sureshkumar, M.D. Smith, R.C. Armstrong, R.A. Brown, Linear stability and dynamic of viscoelastic flows using time-dependent numerical simulations, J. Non-Newtonian Fluid Mech. 82 (1999) 57.
[6] A.M. Grillet, B. Yang, B. Khomami, E. Shaqfeh, Modeling of viscoelastic lid-driven cavity flow using finite element simulations, J. Non-Newtonian Fluid Mech. 88 (1999) 99.
[7] M.C. Navarro, H. Herrero, A.M. Mancho, A. Wathen, Efficient solution of a generalized eigenvalue problem arising in a thermoconvective instability, Commun. Comput. Phys. 3 (2) (2008) 308.
[8] R. Sureshkumar, K. Arora, Efficient computation of the eigenspectrum of viscoelastic flows using submatrix-based transformation of the linearized equations, J. Non-Newtonian Fluid Mech. 104 (2002) 75.
[9] R. Sureshkumar, Stability analysis using compressible viscoelastic formulations, J. Non-Newtonian Fluid Mech. 116 (2004) 471.
[10] M.D. Graham, Effect of axial flow on viscoelastic Taylor–Couette instability, J. Fluid Mech. 360 (1998) 341.
[11] R. Kupferman, On the linear stability of a plane Couette flow for an Oldroid-B fluid and its numerical approximation, J. Non-Newtonian Fluid Mech. 127 (2005) 169.
[12] K.N. Christodoulou, L.E. Scriven, Finding leading modes of a viscous free surface flow: an asymmetric generalized eigenproblem, J. Sci. Comput. 03 (1988) 355.
[13] J.V. Valério, M.S. Carvalho, C. Tomei, Filtering the eigenvalues at infinity from the linear stability analysis of incompressible flows, J. Comput. Phys. 227 (2007) 229.
[14] M.J. Szady, T.R. Salomon, A.W. Liu, D.E. Bornside, R.C. Armstrong, R.A. Brown, A new mixed finite element method for viscoelastic flows governed by diferential contitutive equations, J. Non-Newtonian Fluid Mech. 59 (1995) 215.
[15] M. Pasquali, L.E. Scriven, Free surface flows of polymer solutions with models based on the conformation tensor, J. Non-Newtonian Fluid Mech. 108 (2002) 363.